Top Curr Chem (2011) 304: 153–169
DOI: 10.1007/128_2011_142

Published online: 27 April 2011

A Nanomembrane-Based Nucleic Acid Sensing Platform for Portable Diagnostics

Satyajyoti Senapati, Sagnik Basuray, Zdenek Slouka, Li-Jing Cheng, and Hsueh-Chia Chang

Abstract In this perspective article, we introduce a potentially transformative DNA/RNA detection technology that promises to replace DNA microarray and real-time PCR for field applications. It represents a new microfluidic technology that fully exploits the small spatial dimensions of a biochip and some new phenomena unique to the micro- and nanoscales. More specifically, it satisfies all the requisites for portable on-field applications: fast, small, sensitive, selective, robust, label- and reagent-free, economical to produce, and possibly PCR-free. We discuss the mechanisms behind the technology and introduce some preliminary designs, test results, and prototypes.

Keywords Depletion · Dielectrophoresis · Ion-selective membranes · Limiting-current

Contents

S. Senapati, S. Basuray, Z. Slouka, L.-J. Cheng, and H.-C. Chang (✉)
Department of Chemical and Biomolecular Engineering, University of Notre Dame, 46556 Notre Dame, IN, USA
e-mail: hchang@nd.edu

Abbreviations

AC	Alternating current
CNT	Carbon nanotube
DC	Direct current
DEP	Dielectrophoresis
DNA	Deoxyribonucleic acid
FCW	Fluorescence correlation spectroscopy
FET	Field-effect transistor
I–V	Current–Voltage
kb	Kilobase
PCR	Polymerase chain reaction
pM	Picomolar
RNA	Ribonucleic acid
SNP	Single-nucleotide polymorphism
ssDNA	Single-stranded DNA

1 Introduction

A new molecular sensing platform promises to significantly advance existing electrochemical/capacitance/field-effect transistor (FET) sensing technology into a probe-functionalized, multitarget and smart (automated) electrode sensing platform, whose assay time (minutes), detection limit (picomolar concentrations), selectivity (single-base mismatch discrimination), dynamic range, and robustness are orders of magnitude better than the current state-of-the-art techniques. The platform involves no moving parts, no valves, no optical detection, and will be fully automated with regenerable probes for prolonged usage. Most importantly, the assay time is shorter than the hour-long degradation half-life of RNAs, enabling realization of a polymerase chain reaction (PCR)-free nucleic acid detection platform [1]. The new DNA/RNA sensing technology is based on several new on-chip ion-selective membrane and nanoslot technologies developed in our group and elsewhere [2–7].

Development of rapid and portable detection devices for point-of-care application is an important aspect of the modern diagnostics industry for effective detection of diseases in developing countries, from anti-terrorism and biowarfare applications to environmental monitoring, including the detection of harmful organisms on beaches. The most specific sensing platform is the genetic detection platform, which identifies a particular sequence of the target pathogen's genome. As a result of active research in this area, small pretreatment units are now available that can concentrate the pathogens with membranes and beads, lyse cells, and remove chromosomal DNA for amplification in an integrated PCR chip [8].

However, the key technological bottleneck remains the detection and quantification of the amplified DNAs.

Two gold standards for genetic detection have appeared in the last decade, both involving labeling of fluorophores or quenchers onto the target molecule during PCR amplification: DNA microarray and real-time PCR. DNA microarrays offer sensitivity and large library volume. However, the assay time is long due to diffusion limitations. It also requires periodic rinsing to avoid nonspecific binding. Finally, the fluorescent confocal detection instrumentation is still too bulky and costly for portable applications. Quantification of the number of target DNAs is also impossible. Real-time PCR sacrifices large library volume for rapid and quantifiable detection, higher sensitivity, and good selectivity. However, it still requires expensive and bulky fluorescent detection instrumentation. (Model ViiA^{TM}7 of Applied Biosystems is the size of a small refrigerator and costs US $200,000.) The main challenge for portable diagnostics is then a miniature label-free nucleic acid sensing platform without any sophisticated instruments and reagents. The elimination of the PCR step would also be advantageous, as it would remove the 30-min thermal cycling time and the need for a PCR unit. In many medical applications, over a million DNA and RNA copies are available in a typical sample volume of 100 μL. Consequently, a detection platform capable of sensing one million copies of DNA/RNA can be PCR-free. For bacterial pathogens, each cell produces a million copies of mRNA and only one copy of DNA. However, the tradeoff for this relative abundance of RNA is its short life-time (less than an hour) due to rapid degradation [1]. Hence, an RNA detection platform with an assay time of less than 1 h (and without reverse-transcription PCR) would be the first RNA detection platform of its kind.

Several label-free field-use DNA/RNA sensing technologies have been intensively studied in the last decade. The most viable field-use sensing technology to date is, in our opinion, electrochemical sensing. Electrochemical sensing with molecular probe functionalized electrode sensors can measure the change in electron-transfer rate upon docking of the target DNA/RNA molecules and redox reporter agents that can magnify this electrochemical current. Because many current carriers and inhibitors in the buffer can affect this electrochemical signal, even in the presence of surface-assembled monolayers, this sensing technology lacks robustness and is difficult to calibrate [9]. Capacitance, conductance, and FET electrode sensors have also attracted considerable interest recently. For such non-Faradaic sensors, excess charges brought to the surface by the docked DNA/RNA molecules and their associated potential can produce a local change in Debye double-layer conductance/capacitance and sub-surface current of the sensor. Conductance measurements are typically insensitive at practical ionic strengths because the presence of the DNA/RNA molecules in the high-conductivity Debye layer would not significantly affect the local conductance [10, 11]. Moreover, the same Debye layer is only a few nanometers thick for practical RNA samples, and only the lower fraction of the charges on the long (>10 kb) linear DNA/RNA is responsible for the capacitance signal, again resulting in low sensitivity [12, 13]. At its current state, conductance/capacitance/FET sensors have a

detection limit higher than nanomolar, which translates into 10^8 copies of nucleic acid molecules for practical sample volumes [13], which is too high for field-based detection. Most importantly, the largest drawback of all electrode sensors is their long assay time. At the low target molecule concentrations (picomolar) of practical samples, the diffusion time of long (more than kilobase) nucleic acids to the electrode sensor often exceeds hours, thus rendering such a platform ineffective for rapidly degrading RNA.

Several techniques have been suggested for removing the slow transport of long nucleic acid molecules to the electrode sensor. One technique involves the activation of a high voltage at the electrode sensor to electrophoretically attract nearby DNAs [14]. However, this electrophoretic concentration technique is highly nonspecific and other like-charge molecules can also be attracted to the sensor. Moreover, for buffers of high ionic strength, the elevated voltage can produce undesirable Faradaic reactions that can produce false current or voltage signals. Internal vortices, generated on microelectrodes by various ingenious but unreliable mechanisms, have also been suggested as a means of concentrating the target molecules towards the sensor [15, 16]. Generation of internal vortices remains, however, an imperfect science. It would be more desirable for the sensor to generate such vortices automatically at a precise location and for the vortices to exhibit a strong electric signal such that they can be detected and automatically controlled; this new technology will be described in Sect. 2.

The missing technologies for portable DNA/RNA diagnostics are therefore a label-free electrode sensor that does not suffer from diffusion limitation (i.e., short assay time), is highly selective and sensitive, and yet is insensitive to buffer ionic strength and chemical composition. We propose here that the ion-selective membrane sensor technologies, with properly tuned electrokinetic features and dynamic feedback actuation, can meet these specifications. Our group has recently developed an on-chip sol–gel silica fabrication technique [17, 18] and a nanocolloid assembly technique for on-chip membrane synthesis [3]. We have also applied several photocuring polystyrene sulfonate or polyallylamine synthesis techniques to fabricate on-chip membranes [19]. Recently, we have developed the technology to fabricate nanoslots on chips [5], which behave like single-pore membranes, for application in diagnostic chips. The membranes are used for molecular detection and involve continuous pumping of the sample solution in a cross-flow (tangential to the membrane surface) format to minimize hydrodynamic resistance. On-chip electrodes control the ionic current and voltage drop across these membrane components to produce the desired phenomena for rapid molecular concentration, transport, and detection. A first-generation integrated chip is shown in Fig. 1 for rapid detection of kilobase DNA with probe-functionalized nanocolloid assemblies (membranes). These passive chips are not automated and do not involve feedback control because they are missing several sensors and activation components that our group has recently developed. We will discuss our recent attempts to add and integrate, via on-chip feedback control circuitry, these new components to the first-generation devices to produce a multitarget smart DNA/RNA sensor platform.

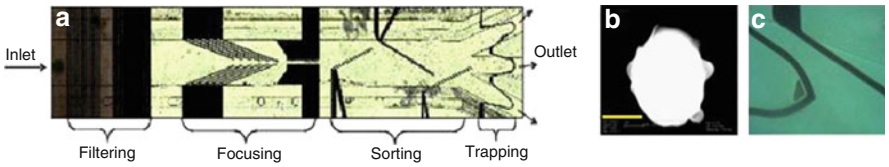

Fig. 1 (**a**) Open-flow DEP chip through which nanocolloids functionalized with complementary oligonucleotides are pumped. (**b**) SEM image of a larger colloid (500 nm) with a long oligonucleotide. *Scale bar*: 200 nm. These nanocolloids are focused, sorted and assembled passively at a microelectrode gate with symmetric and aligned top-down electrode pairs. (**c**) Magnification of a microelectrode gate; the *triangle* shows the trapping of nanocolloids within a micrometer-sized region. DNA solutions, ranging from picomolar to nanomolar concentrations, are then pumped over the nanocolloid assembly (membrane). Fluorescent imaging (see Fig. 6) is used to quantify the specificity and concentration factor, whereas label-free detection yields quantifiable electrical signals (see Figs. 4, 8 and 10)

2 Membrane-Induced Deionzation, Debye Layer Extension, and Induced Vortex Molecular Concentration

One solution to the robustness issue is to deplete the inhibitors and chemicals around the sensor such that close to deionized water conditions are always produced near the sensor, regardless of the buffer ionic strength and composition. Our laboratory has recently developed several of these depletion technologies based on fabricated ion-selective nanoslots [5–7] and on-chip nanoporous membranes [17, 18]. Significant counterion transport can rapidly deplete the counterions on one side of the membrane. To sustain electroneutrality, the co-ions also deplete rapidly to produce an ion-depleted zone. Sufficiently high DC fields (>100 V/cm) can deionize a 100 μm neighborhood (the depletion zone) near the membrane. The depletion layer with low interfacial ionic strength produces the maximum possible ion current without convection and exhibits a distinct limiting-current plateau in the polarization *I–V* or cyclic voltammetry spectrum (Fig. 2b). This nonlinear *I–V* polarization is not due to electron-transfer reactions but bulk-to-membrane ion flux across the extended and depleted interfacial double layer. Its sensitivity to the interfacial charge in the depleted double layer allows sensitive conduction/capacitance detection of hybridization with the same actuation on-chip electrodes that drive the ion current.

At another critical voltage, the limiting current gives way to a sharp increase in the current, the overlimiting current, which is a very sensitive signature of vortices driven by an extended polarized (Debye) layer at the membrane interface, as shown in Fig. 2b [4, 10, 20]. Nonequilibrium (counter)ion transport across the ion-selective membrane produces an extended polarized layer and nonequilibrium over-potential that is orders of magnitude thicker/higher than the Debye screening length and the equilibrium zeta-potential. As such field-induced polarization is curvature- and perturbation-sensitive, the induced electro-osmotic flow is not uniform and the resulting backpressure can drive microvortices of specific dimension, and linear velocity at

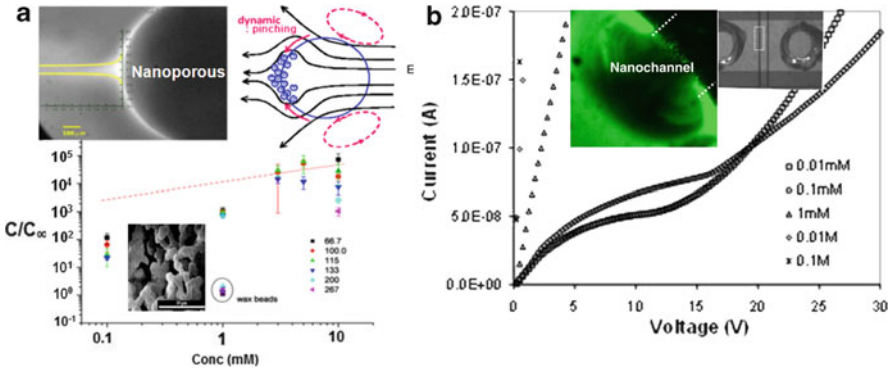

Fig. 2 (**a**) Enrichment and depletion across a nanoporous silica granule synthesized within a glass chip by sol–gel chemistry, producing a five orders of magnitude concentration of ions on one side of the granule and a comparable degree of ion depletion on the other side. *Top left*: High magnification SEM image of silica granule with superimposed plot showing ion concentration. *Top right*: Scheme illustrating counterion movement. *Bottom*: Concentration factor c/c_∞ as a function of the ionic concentration (c_∞) of the fluorescent solution for different sizes of silica beads. *Inset*: SEM image of silica beads. (**b**) Depletion of charged fluorescent dye (*left image*) at one entrance of a 50 nm nanoslot between two circular microreservoirs (*right image*). The depletion has a very distinct polarization signature: the current plateaus at a limiting current value when depletion occurs. When vortices are observed in both the silica granule and the nanoslot beyond a critical voltage, the polarization (single-sweep cyclic voltammetry) curve shows a large overlimiting current beyond the limiting current plateau. The same overlimiting current is shown in Fig. 4 before and after hybridization. The plot shows the polarization characteristics of the nanoslot for different ionic concentrations of solution. Linear polarization curves missing the limiting region can be observed for concentrations above 0.1 mM. The disappearance of the limiting region is given by the loss of the ion-selective properties of the nanochannel as a result of decreasing Debye layer thickness inside the nanochannel

precise voltage windows. Such microvortices enhance the ion current through the membrane or nanoslot (hence the overlimiting current) and thus exhibit a sensitive polarization or single-sweep cyclic-voltammetry overlimiting signal as shown in the polarization curve in Fig. 2b. This strong conductance signature allows us to develop a smart platform that can generate such vortices on demand. Concentration of the charged dye by five orders of magnitude (shown in Fig. 2a) is mostly due to convective concentration of the molecules at the stagnation points of the vortices. Other than the distinctive conductance signals of the membrane depletion/vortex phenomena, their actuation and sensing time is also very rapid. With thin membranes and short nanoslots (Fig. 2b), the ion depletion and hydrodynamic timescales range from microseconds to seconds, allowing for rapid automation.

The ion current across an ion-selective medium can be very sensitive to the charge polarity and density on the surface outside the medium. Our previous work on alumina nanochannels demonstrates that with negatively charged SiO_2 entrance side-walls, the ion conductance across the positive-charged Al_2O_3 nanochannel is suppressed and shows a nonlinear *I–V* characteristic (Fig. 3a). The ion charge inversion induced by the heterogeneous entrance charge enhances ion depletion

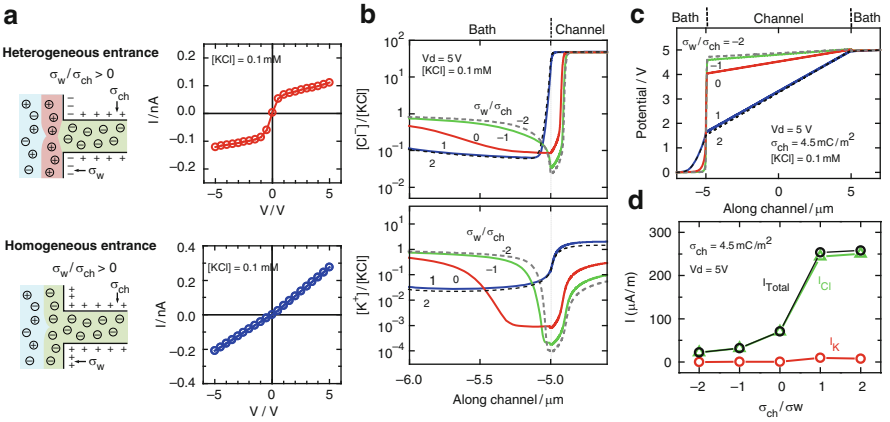

Fig. 3 Effect of entrance surface charge density and polarity on the ion transport in a 20 nm thick, 60 μm long, positively charged Al_2O_3 nanochannel. (**a**) Heterogeneous nanochannel entrance (the charge of entrance side-walls, σ_w and the charge of nanochannel σ_{ch} appear in opposite polarities, $\sigma_w/\sigma_{ch} < 0$) induces ion charge inversion at channel access. Experimental *I–V* characteristics of an Al_2O_3 nanochannel device with negatively charged silica entrance side-walls (*top*) and Al_2O_3 entrance side-walls (*bottom*) measured with 0.1 mM KCl. (**b**) Calculated Cl ion and K ion distributions near left channel entrance with values of σ_w/σ_{ch} varying from 2 to −2. (**c**) Calculated potential profile along the nanochannels with varied σ_w/σ_{ch} ($\sigma_{ch} = 4.5$ mC/m^2) under V_d (Voltage applied across the nanochannel) = 5 V. (**d**) Summarized theoretical ion current density (current per channel width) of the nanochannels with varied σ_w/σ_{ch}

(Fig. 3b) and hence creates a large voltage drop at the channel entrance (Fig. 3c). The heterogeneous entrance charge efficiently suppresses the flow of counterions through the nanoslot (anions in the case of the positively charged Al_2O_3 nanochannel). This effect is clearly seen in Fig. 3d and is reflected in the measured *I–V* curves depicted in Fig. 3a. The ion conductance is found to change significantly when the surface charge of the entrance side-walls converts its polarity and density. The shift of ion conductance induced by surface charge conversion will be utilized as a basis of DNA/RNA sensing. Hybridization of DNA or RNA on a positively charged anion-selective medium can be detected by measuring the nonlinear *I–V* characteristics.

3 On-Chip Membrane Synthesis and Functionalization

Another key step is the proper development of surface chemistry to attach addressable probes onto different membrane sensors. This can be achieved by patterning UV-curable acrylic-based polymers inside the microfluidic channel doped with different monomers containing charged or functional groups. Such polymers are ion-selective and provide reactive chemical groups on their surfaces for the attachment of DNA/RNA probes. The functionality of all the devices proposed here relies on the ion-selectivity of the polymeric material, which is less dependent on

ionic strength than the nanofluidic counterparts. Briefly, using photolithographic techniques, cation- and anion-exchange membranes are defined in glass microfluidic channels by crosslinking positively charged diallyldimethylammonium (DADMA) and negatively charged 2-acrylamido-2-methyl-1-propanesulfonic acid (AMPSA) using a crosslinker (*N*, *N*′-methylene bisacrylamide) and photo-initiator. Each membrane has a defined width and length of few tens to hundreds of micrometers, bridging two microfluidic channels that are about 20 μm deep and 20–100 μm wide. The pore size of the nanoporous membrane can be controlled by varying the concentration of the monomers and crosslinker. To achieve surface functionalization of the oligo probes, the surface of an anion-exchange membrane is modified with amino groups by using allylamine as an additive in the prepolymer solution. The DNA or RNA probe (~27 bases) pre-attached with functional groups of choice can then be used to functionalize the probes onto membrane surface. Through examination by microscope and measurement of the ability to deplete ions, the polymerization time and the concentrations of crosslinker and photo-initiator have been optimized to produce reproducible, well-defined ion-selective membranes with functional chemical groups inside microchannels.

In Fig. 4, we show the first experimental evidence that the onset voltage and the onset of overlimiting current, key features of the nonlinear *I–V* curve of our sensor, are sensitive to nucleic acid hybridization onto oligo probes functionalized onto the surface of the ion-selective medium, as the resulting change in the surface charge can enhance or eliminate the extended Debye layer. The voltage differential is particularly large because of the nearly infinite differential resistance at the limiting current conditions. In contrast, the low-voltage linear ohmic region, where classical electrochemical sensors operate, registers an insignificant shift. Most conveniently, the depleted and extended double layer, which can be three orders of magnitude thicker than the Debye layer, also allows more charges on the target RNA to contribute to the effective surface charge. If the membrane is oppositely charged from the hybridized or functionalized molecules, the latter can even invert the charge on the membrane surface, eliminating the overlimiting current completely

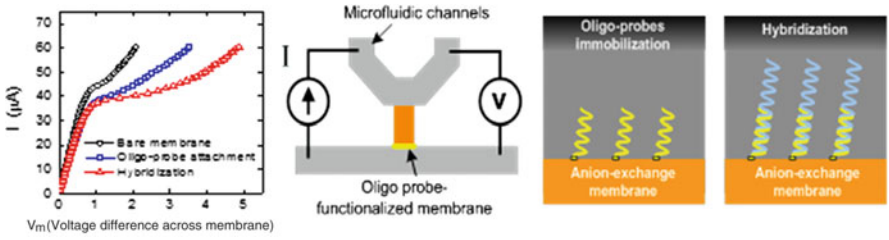

Fig. 4 Ion-selective membrane as a sensitive sensor for the detection of biomolecules. *Left*: Significant change of *I–V* characteristics in the overlimiting current regime is observed after RNA hybridization from a picomolar sample. The 50% change in conductance is compared to typical 5% changes of electrochemical electrode sensors at the same concentration (low-voltage region). *Center*: Diagram of sensor showing position of membrane. *Right*: Schematic presentation of nucleic acid hybridization onto immobilized oligoprobes

when the surface is effective electroneutral with exact compensation. The result is a very sensitive RNA sensor with picomolar sensitivity, compared to the nanomolar sensitivity of most electrode electrochemical sensors, as seen in Fig. 4.

4 Dielectrophoretic and Electrokinetic Molecular Concentration

Dielectrophoresis (DEP), a molecular force due to induced molecular dipoles, has been shown to be an effective means of concentrating large DNA/RNA molecules into the depleted region near the membrane surface (see Figs. 3, 4) where the probes are functionalized [9–12]. The electric field is focused by the nanopores in the membrane to produce a high field gradient at the membrane interface. A polarizable molecule in the bulk, with a large induced dipole, would then experience a net force towards the high-field region (the membrane surface). With the intense field amplification of nanopores, this DEP force on the molecules can overcome molecule–membrane repulsive interaction.

In a recent fluorescent correlation spectroscopy (FCS) experiment in collaboration with Yingxi Elaine Zhu (University of Notre Dame), our laboratory was able to confirm this domination of dielectrophoretic attraction over like-charge repulsion with floating probe-functionalized carbon nanotubes (CNTs) and the fluorescently labeled kilobase target single-stranded DNA (ssDNA). Because CNTs quench the fluorophores on hybridization of target DNA, reduction in the fluorescent intensity can be used to quantify the hybridization degree and the attraction of the molecules to the nanoelectrode. As seen in Fig. 5, dielectrophoretic attraction due to the

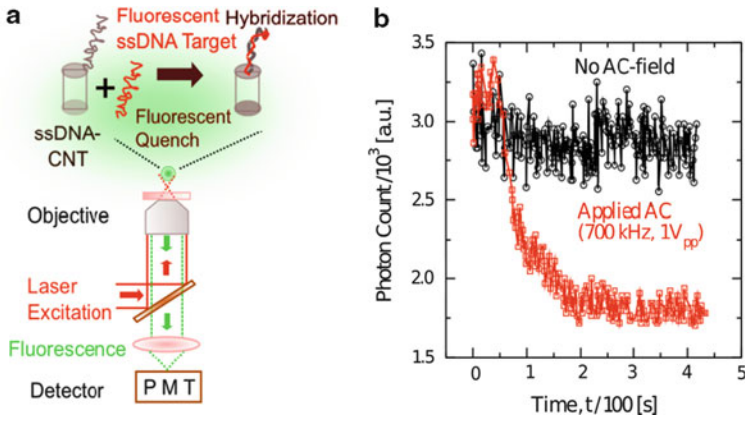

Fig. 5 (**a**) FCS detection of DNA hybridization from a picomolar solution. (**b**) Accelerated DNA fluorescence quench upon DNA docking with oligo-functionalized CNT probe under AC fields, in sharp contrast to the hour-long diffusive docking process without AC-fields

field-focusing CNTs allows hybridization in less than 2 min at picomolar concentrations. In contrast, the diffusion time for the long ssDNA at this concentration is hours.

Instead of floating nanoelectrodes (CNTs), our laboratory [3–7] is able to fabricate 50 nm nanoslots on glass (inset in Fig. 3b) and is able to show concentration of ssDNA to the nanoslot. The same DNA concentration is shown with nanoporous membranes in Fig. 3, with a concentration factor of up to five orders of magnitude. Alternatively, 100 nm nanocolloids can be assembled into a nanocolloid crystal (a membrane) at a top-down electrode pair by nanocolloid DEP (Figs. 1c, 6). The 10 nm spacing between the nanocolloids focuses the electric field of the electrode gate and can rapidly (order of seconds) trap and concentrate ssDNA

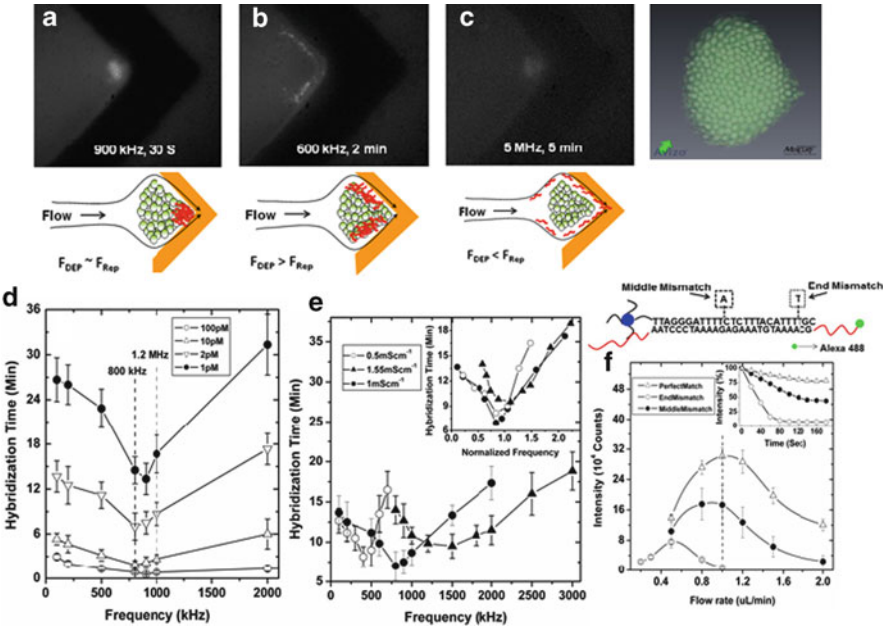

Fig. 6 (**a**–**c**) Fluorescence images of the trapping electrode tip in Fig. 2, showing the 100 nm nanocolloid assembly (see SEM image on the *right*) at fixed times after the Green Crab DNA solution had been injected but at different AC frequencies. The fluorescence is detectable only when the ssDNA is concentrated beyond the micromolar level from the undetectable concentrations (nanomolar to picomolar) of the injected solution. The DNA trapping location is further clarified in the schematics below the images. Trapping at the assembly is achieved at low frequencies, whereas none occurs at high frequencies. F_{DEP} dielectrophoretic force, F_{Rep} repulsive force. (**d**) Detection time increases with decreasing concentration. (**e**) There is an optimum frequency with a sharp minimum in detection time, which scales as D/λ^2 where λ is the Debye length for the given electrolyte strength. (**f**) Fluorescence intensity at 2 min from different flow rates of 100 pM of a 1 kb ssDNA target from a Green Crab species with a 26 base docking segment in the middle (*solid cricle*) and with a complementary 26 base oligo on the nanocolloid (*open triangle*) or with a single end mismatch (*open circle*). The flow rate window with single-mismatch discrimination is indicated by a *vertical dashed line*. The scheme above the plot shows the actual 26 base ssDNA docking sequence and the location of mismatched bases

molecules of a Green Crab species [3] from a picomolar solution onto the on-chip nanocolloid membrane by molecular DEP. A properly tuned DEP force can drive the DNAs towards the nanostructure against electrostatic repulsion from the like-charged structures, but they will not deposit onto the surface until they are convected to a sharp tip (~10 μm) at the nanostructure (Fig. 6a); intermolecular interaction can be adjusted to minimize nonspecific binding. A concentration factor exceeding 10^5 within minutes is observed from the fluorescent imaging in Fig. 6, thus rapidly and significantly enhancing the sensitivity of any sensor at the trapping location. The shear rate and AC frequency can be optimized so that the sensor can selectively discriminate against kilobase target molecules with a single mismatch in the 26 base pairing segment in the middle (Fig. 6f). This shear-enhanced selectivity eliminates the need for rinsing and washing steps.

Apart from dielectrophoretic concentration, which is not effective for small nucleic acids because the DEP force scales as the cubed power of the hydrodynamic radius of the molecule, our group has successfully demonstrated rapid analyte preconcentration based on ion depletion at an ion-selective membrane in microfluidic chips. As shown in Fig. 7a, a cation-exchange membrane UV-polymerized in a microslot bridging two microfluidic channels can induce deionization under voltage biases. The ion-depletion region functioning as an energy barrier traps the molecule passing across it in an electroosmotic flow tangential to the membrane on the side. The UV-curable ion-selective membrane offers superior concentration efficiency and proccessability compared to the microfabricated nanochannels reported previously [21, 22] or Nafion resins [23, 24]. Unlike the 100 nm thick nanochannels and surface-patterned Nafion thin films, the proposed membrane slot has the same depth as the microfluidic channel, yielding a large junction area. The large cross-section area provides greater ion current and better control of ion-depletion in the microchannels. Therefore, preconcentration can be achieved in few seconds. The fluorescence image in Fig. 7b shows the concentration of labeled molecules by several orders of magnitude in 10 s from a solution being pumped by

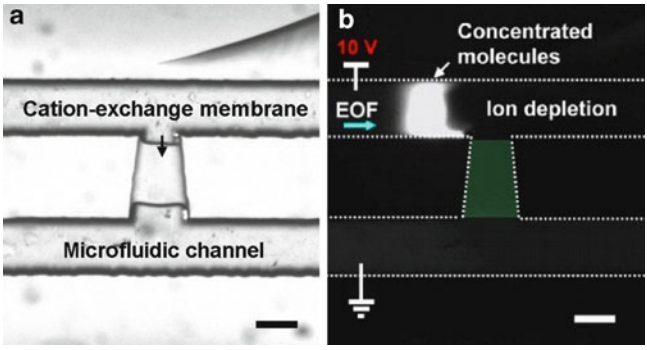

Fig. 7 (**a**) Optical microscopic image of a preconcentrator based on a charge-selective membrane. (**b**) Concentration of fluorescently labeled molecules taking place 10 s after applying a voltage bias of 10 V. Scale bars: 50 μm. *EOF* electroosmotic flow

electro-osmosis from the left to right in the top microfluidic channel, after 10 V is applied across the membrane. Moreover, the proposed membrane adheres to acryl-functionalized glass surfaces well; whereas Nafion has poor adhesion to most solid surfaces and the process is more operator-dependent.

5 Polarization and Warburg Impedance Signals of Membrane Sensors: Label-Free and Non-Optical Detection

The presence of the docked RNA/DNA and their mobile counterions produce a large conductivity change at the depleted region, which is where most of the voltage drop occurs. Moreover, the extended Debye (polarization) layer [4, 25] allows more of the charges on a long (>2 nm) DNA/RNA molecule to contribute to the charging capacitance and surface-charge compensation on the surface. As described earlier, the surface charge can sensitively alter the onset voltage for microvortices and the overlimiting currents that the vortices contribute to. These effects greatly enhance the capacitance, conductance and polarization signatures of the docked nucleic acids, resulting in sensitive nonlinear *I–V* polarization signatures, such as those due to the charge-inversion after hybridization in Fig. 4.

The dynamics of depletion layer formation with strong charging also exhibits a distinct capacitance signature in the AC impedance spectrum (Fig. 8a). This Warburg spectrum has a constant phase angle of π/4, whose modulus increases with decreasing frequency and is classically associated with diffusion controlled ion transport. In a recent paper [7], we have shown that, under an AC field, the depletion region next to a membrane sensor is created periodically during the

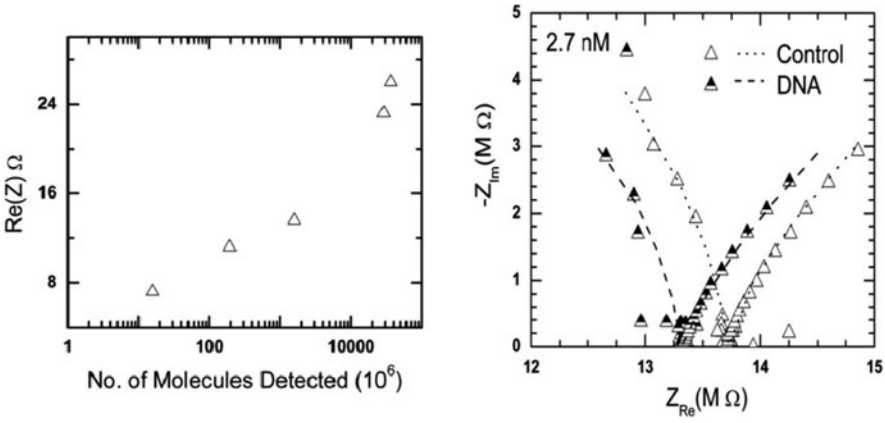

Fig. 8 (**a**) Warburg impedance spectrum of the nanoslot in Fig. 2b, showing a shift to lower resistance with a 2.7 nM 1 kb *E. coli* ssDNA solution relative to the control without DNA. (**b**) The shift in the intercept with the real axis allows precise quantification of the number of ssDNA molecules in the microreservoir down to 10^7 copies

half-cycle when the mobile counterions are driven into the nanoslot or on-chip membrane. The depletion layer dynamics was verified by high-speed confocal imaging to be a diffusive one such that its thickness grows in a self-similar manner as $\sqrt{Dt}$ [5] and was shown to exhibit the Warburg spectrum, with a constant phase of $\pi/4$ (Fig. 8a). The intercept of the Warburg spectrum with the real axis represents the limiting ion flux when the depletion layer is smallest in dimension – just above the critical voltage where the depletion phenomenon can be sustained. It hence offers an accurate estimate of the low conductivity in this small region, as most of the voltage drop occurs there. As mentioned earlier, the presence of a few macro-ions attracted to this small depleted region by DEP can significantly change its local conductance. In Fig. 8b, we indicate sensitive detection of *E. coli* ssDNA below nanomolar concentrations or 10^7 molecules. With a reduction of the nanoslot width, down to the micrometer size of the nanocolloid assembly in Fig. 6, the detection limit is expected to reach below picomolar concentrations or 10^5 copies of nucleic acid. The same Warburg signal can be captured with the field across the nanocolloid assembly of Fig. 6 to allow label-free quantification of the docked DNA/RNAs. This large-voltage AC impedance technique is quite distinct from the classical low-amplitude impedance spectroscopy for electron transfer rates because we induce nonequilibrium ion transport through the ion-selective nanoslot or membrane to produce extended polarized Debye layer and concentration depletion layers.

6 Selectivity Enhancement

The single mismatch (SNP) discrimination capability of the experiment shown in Fig. 6f is due to hydrodynamic shear. In a recent MD project [15], it has been shown that shear is most discriminating because it can meter small thermal-energy-level

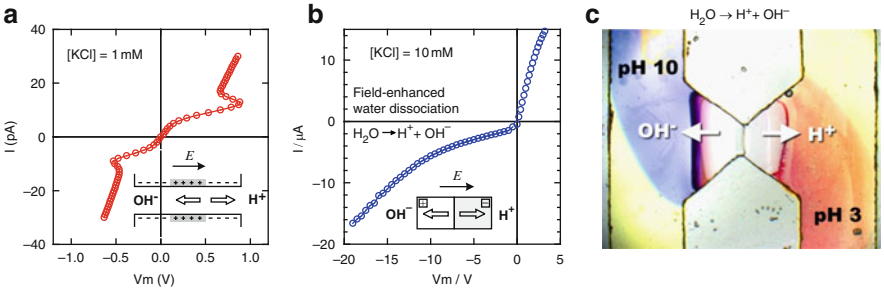

Fig. 9 Field-enhanced water dissociation increases ionic currents in (**a**) a reverse-biased 20 nm thick bipolar-junction nanofluidic channel containing positive and negative surface charges ($|V_m| > 0.6$ V), and (**b**) a UV-polymerized bipolar membrane ($V_m < -10$ V). (**c**) Hydroxide ions and protons are produced at the bipolar membrane junction and transport to opposite sides of the membrane. The pH change of the solution in the microchannels can be observed with a mixture of universal pH indicator. Left half of the bipolar membrane is positively charged whereas the right half is negatively charged

hydrogen bond energies to dehybridize the target molecules. One of the co-authors (S.Z.) and other groups have recently developed microscale bipolar membrane technologies that can be used to control the local pH in microfluidic chips to improve both the specificity and selectivity of the membrane sensor [26, 27]. These bipolar membranes/nanopores exhibit distinct hysteretic *I–V* polarization and cyclic voltammetry signatures due to local field-induced water-breaking reactions that generate more ions [25, 26, 28–30]. An image of the pH fronts generated by a UV-polymerized bipolar membrane composed of positively charged dimethylammonium and negatively charged sulfonic groups are shown in Fig. 9. It was found that the ion currents can drastically increase when reversely biased at a high voltage, forming a breakdown regime. In accordance with the second Wien effect, the ionic current breakdown results from the enhanced water dissociation into cation (H^+) and anion (OH^-) at the bipolar junction, in which a strong electric field greater than 10 MV/cm can build up at a reverse bias [29, 30]. These membrane actuation components can be used to control the local pH for our integrated devices, with feedback control based on the distinctive hysteretic polarization signals and *I–V* characteristics seen in Fig. 9.

7 Integrated Units

Other than the nanoslot chip of Fig. 2 and the DEP chip of Figs. 1, 6 for nanocolloid assemblies, our group has integrated several components into the first-generation of passive sensor chips [2–7]. One prototype is shown in Fig. 10. An assembly of oligo-functionalized CNTs (a CNT membrane) is used to effect the ion depletion and the Warburg quantification (Fig. 8) of hybridized ssDNA from a Green Crab invasive species. The detection limit of the Warburg impedance signal is picomolar concentrations or about the desired 10^5 copies, the detection time is about 15 min,

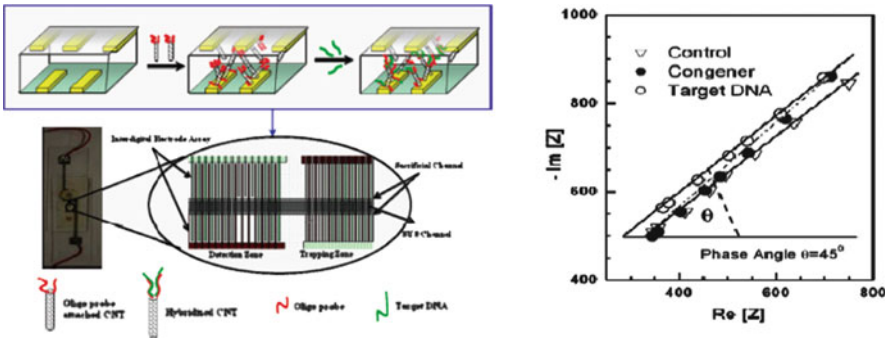

Fig. 10 *Left*: An integrated chip that uses an interdigitated electrode array to assemble oligo-functionalized CNTs into an ion-selective membrane. *Right*: The Warburg signal measured across the CNT assembly is able to detect picomolar concentrations (10^5 copies) of a kilobase-long DNA from a Green Crab species and differentiate a congener species with three mismatches over the 26 pair docking segment due to the hydrodynamic shear offered by the high through flow

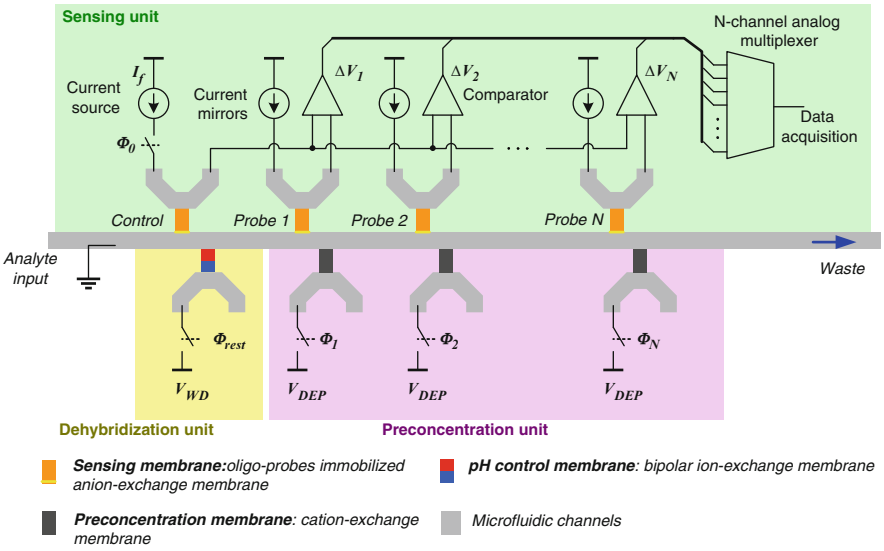

Fig. 11 *Top*: Integrated smart RNA hybridization sensor composed of sensing unit, preconcentration unit, and dehybridization unit. *Bottom*: A functioning prototype measuring 25 × 10 × 40 cm is shown in which a glass chip (like that shown in Fig. 10 but containing the multitarget design) is seen at the top of the instrumentation. A handheld prototype is expected in a year

and the selectivity is three mismatches in the 27 base pairing segments. The study showed that long kilobase target ssDNA produces a larger signal, consistent with the theory that the extended Debye layer allows more of the charges of a long molecule to contribute to the local charge capacitance and conductance.

A multitarget unit currently being developed is shown in Fig. 11. It offers sequential detection of different targets by moving the sample from one sensor

location to the next with the depletion technique. Such a design has been developed for small sample volumes. For larger volumes, a parallel design can be implemented. These multitarget chips and the peripheral instrumentation are being developed by FCubed LLC (http://www.FCubed.iviehost.com). A functioning prototype is shown at the bottom of Fig. 11.

8 Conclusion and Commercialization Issues

Nanoporous membranes can greatly enable and sensitize on-chip molecular sensing. They can deplete inhibitors near their surface where the probes are functionalized, such that the platform is robust to a large variety of sample ionic strengths and pH. More importantly, the same ion-depletion dynamics extends the Debye layer and hence allows more sensitive conductance and capacitance detection of the hybridized molecules. The high field in the same depletion region can produce fast dielectrophoretic trapping of the larger target molecules. If the depletion region extends across the entire flow channel, it can also trap smaller molecules. Hence, by activating different membrane components on a chip, the molecules can be concentrated and transported to different sensors. The membrane's ability to invert its surface charge upon hybridization produces a large conductance signal for hybridization. A large capacitance signal is also produced, corresponding to the intercept of the Warburg spectrum with the real axis, when the depletion layer is formed periodically under an AC field such that the hybridized target molecules and their counterions are responsible for this asymptotic conductance when all other ions are depleted within the small depletion layer. These nanoporous membranes are fabricated on the chip and are situated on the side of the flowing channel without blocking the flow, such that a high throughput (>1 μL/min) can be achieved. Bipolar nanoporous membranes can also be used to split water and to exercise precise control of pH near the sensor, to enhance selectivity. This rapid and precise pH control can also allow multitarget sensing with the same probe if the probes are designed to be pH-sensitive.

Although the current membranes are synthesized on glass chips to allow easy inspection and testing, the same technology can be transferred to hard polymer chips, which should be cheaper to produce and easier to bond. This remains the final obstacle to commercialization.

Acknowledgment The authors are grateful to NSF, Great Lakes Protection Agency, Gates Foundation, NIH and ND-PDT for their generous support of this research.

References

1. Deana A, Celesnik H, Belasco JG (2008) Nature 451:355
2. Basuray S, Senapati S, Ajian A, Mahon AR, Chang H-C (2009) ACS Nano 3:1823
3. Cheng I-F, Senapati S, Cheng X, Basuray S, Chang H-C (2010) Lab Chip 10:828

4. Chang H-C, Yossifon G (2009) Biomicrofluidics 3:012001
5. Yossifon G, Chang H-C (2008) Phys Rev Lett 101:254501
6. Yossifon G, Chang Y-C, Chang H-C (2009) Phys Rev Lett 103:154502
7. Yossifon G, Mushenheim P, Chang Y-C, Chang H-C (2009) Phys Rev E 79:046305
8. Cady NC, Stelick S, Kunnavakkam M, Batt CA (2005) Sens Actuators B 107:332–341
9. Bakker E, Qin Y (2006) Anal Chem 78:3965
10. Umezawa Y, Aoki H (2004) Anal Chem 76:321
11. Basuray S, Chang H-C (2010) Biomicrofluidics 4:013205
12. Suni II (2008) Trends Anal Chem 27:604
13. Stern E, Wagner R, Sigworth FJ, Breaker R, Fahmy TM, Reed MA (2007) Nanolett 7:3405
14. Sosnowski R, Tu E, Butler WF, O'Conell JP, Heller MJ (1997) Proc Natl Acad Sci USA 94:1119
15. Kreft J, Chen YL, Chang H-C (2008) Phys Rev E 77:030801
16. Lin HT, Tsai LC, Chi PY, Chen CD (2005) Nanotechnology 16:2738
17. Wang P, Chen Z, Chang H-C (2006) Sens Actuators 113:500
18. Wang P, Chen Z, Chang H-C (2006) Electrophoresis 27:3964
19. Senapati S, Mahon SR, Gordon J, Nowak C, Sengupta S, Powell THW, Feder J, Lodge DM, Chang H-C (2009) Biomicrofluidics 3:022407
20. Ben Y, Chang H-C (2002) J Fluid Mech 461:229
21. Cheng L-J, Guo LJ (2010) Microfluid Nanofluid 9:1033
22. Wang Y-C, Stevens A, Han J (2005) Anal Chem 77:4293
23. Lee JH, Song Y-A, Han J (2008) Lab Chip 8:596
24. Liu V, Song YAK, Han J (2010) Lab Chip 10:1485
25. Cheng L-J, Guo LJ (2009) ACS Nano 3:575
26. Slouka Z, Pribyl M, Snita D, Postler T (2007) Phys Chem Chem Phys 9:5374
27. Zhang H, Mitrovski SM, Nuzzo RG (2007) Anal Chem 79:9014
28. Onsager L (1934) J Chem Phys 2:559
29. Ramirez P, Manzanares JA, Mafé S (1991) Ber Bunsenges Phys Chem 95:499
30. Mafé S, Manzanares JA, Ramirez P (1990) Phys Rev A 42:6245